Universiteit Utrecht

Opleiding Natuur- en Sterrenkunde

Studies for the early electromagnetic fields at LHC energies

BACHELOR THESIS

Michiel Lugt

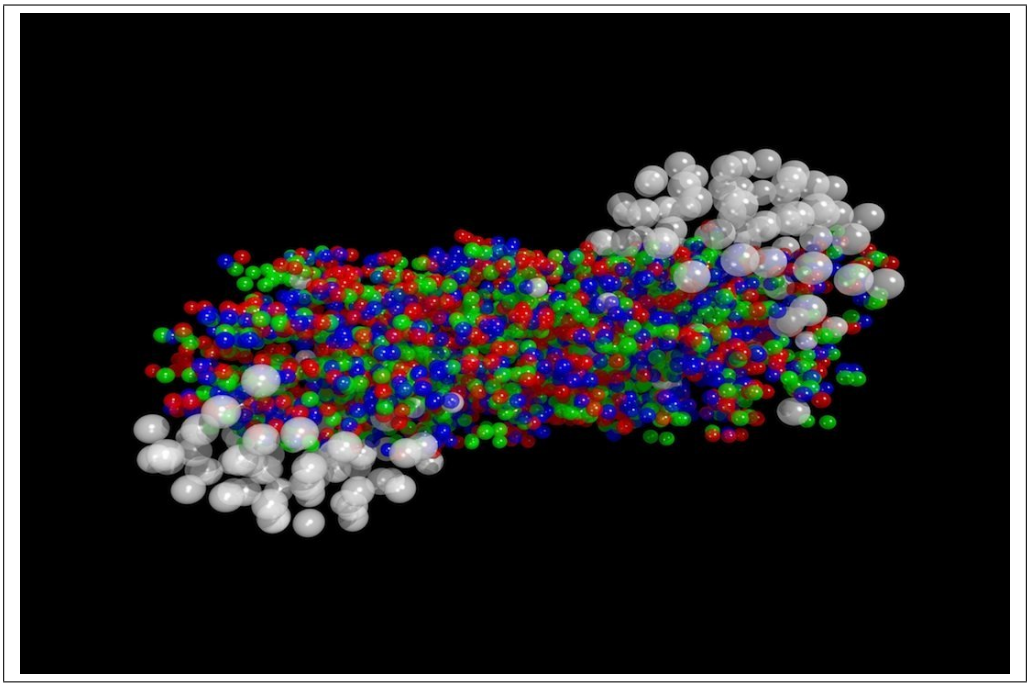

Supervisor:

Dr. P. CHRISTAKOGLOU
Utrecht University, Nikhef

June 16, 2021

Abstract

In subatomic physics, one of the main questions is what happens to matter at extreme temperatures and energy densities. In this thesis, we study the Quark Gluon Plasma (QGP) using heavy-ion collisions. The collisions studied are modelled by the AVFD framework. The expansion of the QGP is described by the elliptic flow and the triangular flow. We calculate these flow coefficients for Pb-Pb collision at $\sqrt{s_{NN}} = 5.02$ TeV for various centrality intervals. The goal of the project is to identify signals of the early stage magnetic field in the motion of final state particles. An adequate probe proposed by theory is the elliptic and triangular flow of different charges. The flow of positive and negative charges is determined separately and the ratio is plotted as a function of centrality. We find that for 2 and 4 particle correlations of elliptic flow, and for 2 particle correlations of triangular flow, the flow of the positive and negative charges are not compatible. These differences have been related to the magnetic field induced by the spectator nucleons.

Acknowledgements

I wish to thank my supervisor Panos Christakoglou for all this help and guidance throughout the project.

Contents

1 Introduction **1**

2 Electromagnetic Mechanisms **3**
2.1 Parameters of a collision 3
2.2 Electromagnetic fields 4

3 Hydrodynamical Quantities **7**
3.1 Analysis Flow 8

4 The AVFD model **9**

5 Results **11**
5.1 Results Elliptic Flow v_2 11
5.2 Results Triangular Flow v_3 16

6 Conclusion **19**

1 Introduction

Quantum Chromodynamics (QCD) is the underlying theory of the strong force, which describes the interactions between quarks and gluons. Physicists have been studying the composition of particles and strong interactions for about 50 years. In these years, a theory has been developed that seems to describe the interactions between the quarks and gluons quite well. An excellent testing ground of QCD at extreme values of temperatures and energy densities is provided by heavy-ion collisions. In these collisions, large magnetic fields are produced, high temperatures are measured and phase transitions occur from quarks and gluons into hadrons. At BNL and at CERN, two heavy-ion colliders called the Relativistic Heavy-Ion Collider (RHIC) and the Large Hadron Collider (LHC) can be found. However, the phase transition between the quarks and gluons from their deconfined state to particles composed of quarks and gluons called hadrons (i.e. protons, neutrons, pions), has been a challenge to include into the theory. In heavy-ion collisions, due to the high energies, a so called Quark-Gluon Plasma (QGP) is created. The QGP has first been discovered at the Super Proton Synchrotron (SPS), and has been studied in more detail at RHIC and LHC. Still, its precise properties are yet to be established [1]. The study of QGP draws information from QCD, thermal field theory, electromagnetism, hydrodynamics and quantum collision theory. Shortly after the Big Bang ($\sim 10\ \mu s$) , the universe was a Quark-Gluon Plasma, reaching temperatures $T \gtrsim 200 \cdot 10^{10}$ K. It is hypothesised that the universe was in this state for several microseconds after the Big Bang and that this state may be present in the core of neutron stars [2]. At RHIC and LHC, physicists try to reproduce the QGP in order to get a better understanding for this state and the implications of QCD. A simple drawing of a heavy-ion collision is shown in figure 1. An experiment currently being worked on at CERN that reproduces this plasma is called ALICE (acronym for A Large Ion Collider Experiment).

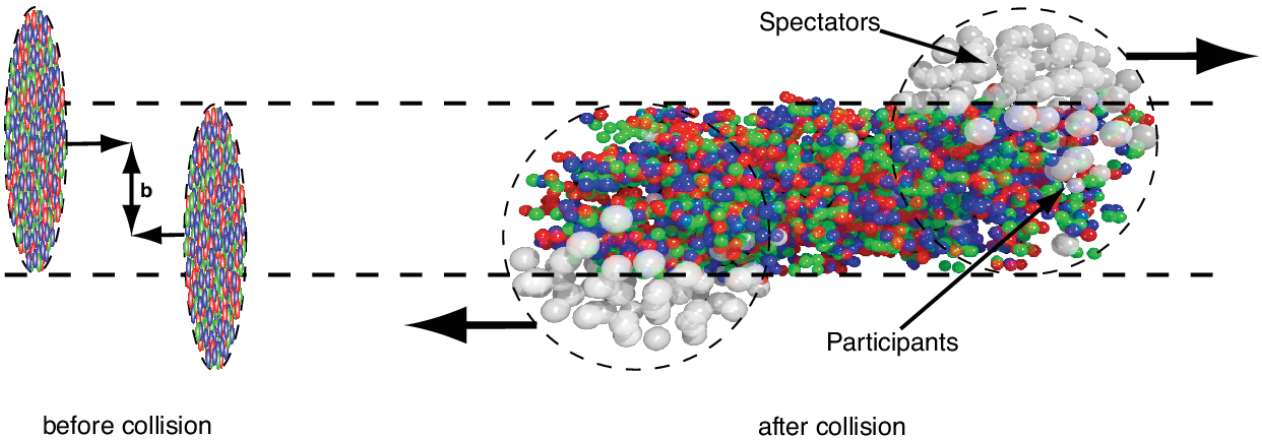

Figure 1: Two heavy ions before and after the collision. Before the collision, the Lorentz-contracted bulks of neutrons are shown with impact parameter b. After the collision, the participants are coloured and interact. The spectators will move past the interaction volume. The figure is taken from Ref. [2].

Through the study of such heavy-ion collisions at both RHIC and the LHC, scientists came to realise that the QGP behaves as a dense, perfect liquid with extremely large temperatures. The study of

anisotropic flow played a crucial role in this conclusion. Anisotropic flow describes the final state momentum anisotropy, which is a reflection of the initial state, in space momentum anisotropy. It is ususally quantified by a Fourier series of the azimuthal angle ϕ particle distribution:

$$\frac{\mathrm{d}N}{\mathrm{d}\phi} \approx 1 + 2\sum_{n} \left(v_n \cos\left[n\left(\phi - \Psi_n\right)\right]\right), \tag{1}$$

where v_n are the *flow harmonics*. v_1 is labeled *directed flow*, followed by v_2 as *elliptic flow*, and v_3 as *triangular flow*.

It was recently realised that heavy-ion collisions possess other intriguing effects, which are not easily accessible in other places. One of these effects is the extreme electromagnetic field that develops in the early stages of a collision. This field is mainly produced by particles that do not participate in the collision, called *spectators*. Using the Biot-Savart law from electromagnetism, one can calculate that the magnetic fields at center-of-mass for collisions at the LHC can reach values of 10^{16} Tesla [3]. This electromagnetic field decays rapidly, with a value that depends on the electric conductivity of the QGP. This parameter is experimentally fully unconstrained. Depending on the value of the conductivity, the initial stage electromagnetic field can have direct implications to the motion of final state particles.

The goal of this project was to illustrate how this extreme field could affect the motion of hadrons produced in such heavy-ion collisions. This was studied with the help of a model, called Anomalous Viscous Fluid Dynamics (AVFD) [4]. This model attempts to describe the various stages of a heavy-ion collision. The document is organised as follows: in chapter 2, the electromagnetic fields and the time evolution of these fields will be discussed. Chapter 3 then examines the flow harmonics v_2 and v_3, followed by an explanation of the geometry of a collision. The AVFD model will be described in chapter 4, after which the results are presented in chapter 5.

2 Electromagnetic Mechanisms

2.1 Parameters of a collision

In this thesis, a collection of parameters corresponding to a collision will be used regularly. When two ions moving in the z-direction collide, a straight line can be drawn from core to core, spanning a plane with the x-axis. This plane is called the *reaction plane*, and is denoted by Ψ_{RP}. The coordinate system is set in the laboratory frame. The impact parameter b is the distance between the two cores of the ions. If the impact parameter is zero, a collision is called *central*. If the impact parameter is large (for example $0.5 \times radius$), a collision is called *peripheral*. A second way to quantify the vertical distance is by using the dimensionless *centrality*. The centrality is characterised by the fraction $\pi b^2/\pi \left(2R_A\right)^2$, of the geometrical cross-section, with R_A the nuclear radius [2]. All incoming nucleons have a momentum, but not all particles collide. The nucleons that participate in the collision are called the participants, the particles that fly past the collision are called the spectators. The volume in which the participants interact will be referred to as the *interaction volume*. All these are depicted in figure 1. The geometry of the interaction volume will be discussed in chapter 3. After the collision, a QGP is created if the necessary conditions are met. The QGP then expands outwards and during this process, its temperature reduces. Once the temperature reaches a value of around 155 MeV, which is called the freeze-out temperature T_f, the QGP starts to hadronize. It will emit the known hadrons, such as pions, kaons, protons and their antiparticles. These particles have some momentum both in the longitudinal and in the transverse direction. The *transverse momentum* p_t is the latter. It is defined as the component of the momentum transverse (or perpendicular) to the beam line. Spectators have zero transverse momentum, as these particles follow the beam line after the collision. The mathematical definition is $p_t = p \sin\theta$, where p is the total momentum of a particle, and θ the particle emission angle, both from the frame of the stationary source. The next quantity is called *pseudorapidity* and is denoted by η. Pseudorapidity describes the angle of the particle relative to the z-axis (beam axis). The corresponding formula is $\eta = -\ln\left(\tan\left(\theta/2\right)\right)$. The *azimuthal angle* ϕ is the angle of an outgoing particle measured from the x-axis. The coordinate system is shown in figure 2 for a noncentral collision (i.e. a collision with impact parameter unequal to zero).

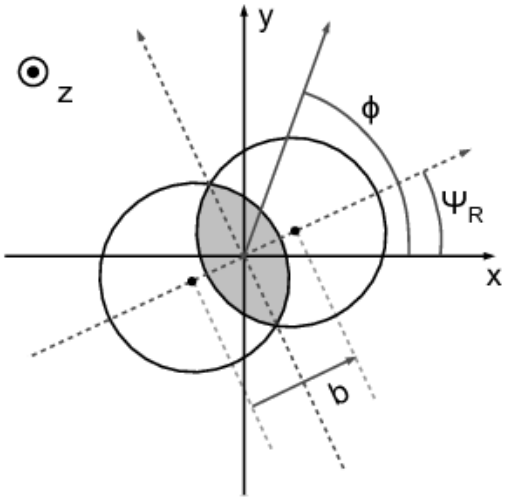

Figure 2: Two particles moving in the z-direction collide. The definitions of impact parameter b, azimuthal angle ϕ, and reaction plane Ψ_{RP} (here Ψ_R) are illustrated. The darkened area represents the interaction volume. The figure is taken from Ref. [5].

2.2 Electromagnetic fields

In heavy ion collisions, large magnetic fields $\vec{B}$ are produced. These magnetic fields arise from multiple sources from both inside and outside the interaction volume. Inside the interaction volume, the charged moving particles produce moving electric fields, inducing magnetic fields. For noncentral collisions (that is nonzero impact parameter), the nucleons that do not participate, i.e. charged spectator nucleons, produce a large magnetic field. An estimate obtained by applying the Biot-Savart law to collisions with an impact parameter $b = 4$ fm yield $e|\vec{b}|/m_\pi^2 \approx 1 - 3$ about $0.1 - 0.2$ fm/c after a RHIC collision with $\sqrt{s_{NN}} = 200$ GeV [3, 6]. Here, $\sqrt{s_{NN}}$ is the center of mass energy of the collision between the two ions. This estimate yields a magnetic field of order 10^{15} T. After the collision, the QGP is formed with a positive net charge. The electromagnetic fields that arise in the collision can be described using the Lorentz force law and the Maxwell equations. The different sources are:

1. Faraday's law. The QGP contains moving charges, inducing an electric field $\vec{E}_F$ and an electric current. As time progresses, $\vec{B}$ decreases and Faraday's law starts to dominate. The direction of the electric field is perpendicular to $\vec{B}$ and in positive x-direction for positive z, and for negative z in the negative x-direction, as illustrated in figure 3.

2. Lorentz force law. The QGP expands outwards with velocity field $\vec{u}$ along the beam direction. The combination of this velocity and the magnetic field result in a Lorentz force on the charged particles. We label the electric field corresponding to this force as $\vec{E}_L$.

3. Coulomb force. The charged spectator particles exert a Coulomb force on the particles in the interaction volume. The direction of this electric field $\vec{E}_C$ is in opposite directions at opposite

rapidity [6].

4. The Quark Gluon Plasma. Although the QGP is not an electromagnetic force, it needs to be included in this list. The QGP generates a sideways current, as the electromagnetic forces and laws above do. The origin for this current is the outwards expansion of the plasma, since the net charge is positive. The corresponding electric field is labelled by $\vec{E}_P$.

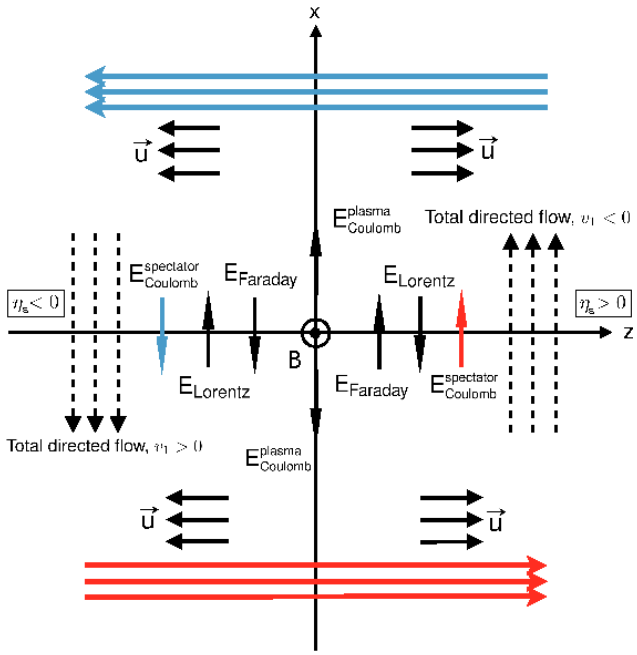

Figure 3: The electromagnetic forces are shown in the xz-plane. The figure is from Ref. [6].

All electromagnetic mechanisms above induce an electromagnetic current. The first three laws/forces induce the direct current v_1. The fourth delivers a contribution to the elliptic flow v_2 through a charge-odd, rapidity-even sideways current.
The time evolution of the electromagnetic fields are described by Maxwell equations

$$\frac{\partial \vec{B}}{\partial t} = -\vec{\nabla} \times \vec{E}, \tag{2}$$

$$\frac{\partial \vec{E}}{\partial t} = \vec{\nabla} \times \vec{B} - \vec{j}, \tag{3}$$

where $\vec{j}$ is the electromagnetic current. In the matter rest frame, the internal current may include the contribution from the Ohmic conductivity

$$\vec{j}_{Ohm} = \sigma_{Ohm}\vec{E} \tag{4}$$

and the one induced by the QED anomaly

$$\vec{j}_{anom} = \sigma_\chi \vec{B}, \tag{5}$$

where $\sigma_\chi \propto \mu_5$ and μ_5 is the axial chemical potential [7]. In equation 4, σ_{Ohm} is the electric conductivity, which has a large contribution to the time evolution of the magnetic field. In figure 4, the magnetic field scaled by the elementary charge and the mass of a pion is plot as a function of time scaled by the radius of a gold ion. The magnitude of the magnetic field decreases rapidly for $\sigma_{Ohm} = 0$ and hardly decreases for large σ_{Ohm}. Here, σ_{LQCD} is the electric conductivity found by the quenched approximation used in Ref. [8].

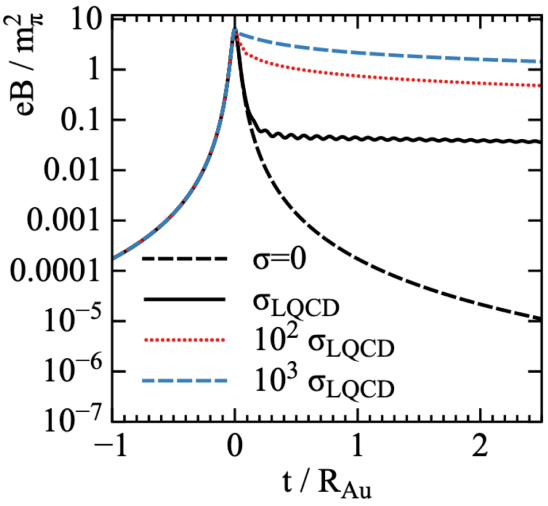

Figure 4: The magnetic field is plotted as a function of time for four different electric conductivities. The figure is from Ref. [7].

3 Hydrodynamical Quantities

At extreme temperatures, we expect that the quarks and gluons are weakly interacting and the QGP would behave as an ideal gas [2]. For this ideal massless gas, the equation of state is given by

$$P = \frac{1}{3}\epsilon, \quad \epsilon = g\frac{\pi^2}{30}T^4, \tag{6}$$

where ϵ is the energy density, g the number of degrees of freedom, T the temperature and P the pressure. The elliptic and triangular flow arise from the Fourier expansion of the particle spectrum. This spectrum is given by

$$E\frac{\mathrm{d}^3N}{\mathrm{d}^3p} = \frac{1}{2\pi}\frac{\mathrm{d}^2N}{p_T\mathrm{d}p_T\mathrm{d}y}\Big(1 + 2\sum_{n=1}^{\infty} v_n \cos\left[n\left(\phi - \Psi_{RP}\right)\right]\Big), \tag{7}$$

where E is the energy of a particle, N the number of particles, p the momentum of a particles, p_T the transverse momentum, y the rapidity, Ψ_{RP} the angle of the reaction plane, and ϕ the azimuthal angle [2]. In this expansion, the coefficients v_n describe physical properties of the fluid. v_1, v_2, and v_3 respectively are called directed, elliptic, and triangular flow. These coefficients explain the anisotropical expansion of the QGP. Namely, the QGP expands more along the short axis than the long axis. The values of these coefficients are determined by

$$v_n(p_t, y) = \langle \cos\left[n\left(\phi - \Psi_{RP}\right)\right]\rangle. \tag{8}$$

Here, the average is taken over all events. A second common expansion to obtain the flow coefficients is the azimuthal distribution of the finally observed charged hadrons particles in the momentum space [9],

$$\frac{\mathrm{d}N^{\pm}}{\mathrm{d}\phi} \propto 1 + 2v_2\cos(2(\phi - \Psi_{RP})) + 2v_3\cos(3(\phi - \Psi_{RP})) + \ldots, \tag{9}$$

The flow coefficients are strongly related to the geometry of the collision. An expansion can be made from the interaction volume. That is, the first term will be a circle, the second term an ellipse with eccentricity ϵ_2, the third term a triangle with 'eccentricity' (the deformation from an equilateral triangle) ϵ_3, the fourth term a square and so on. A combination of all shapes will give an approximation of the interaction volume. For central collisions, the interaction volume is nearly a sphere, yet not be perfectly symmetric. Event fluctuations due to the uncertainty of the position and momentum of the particles will not permit perfect symmetry. Thus for central collisions, all shapes other than the first order sphere are nearly zero. As the collisions become more peripheral, the eccentricities ϵ_2, ϵ_3, ... will increase, as the interaction volume will take the form of an ellipse or a more abstract shape. In general, the elliptic flow has the greatest value, followed by triangular flow, and so on. The eccentricity ϵ_2 is defined as

$$\epsilon_2 = \left\langle \frac{y^2 - x^2}{y^2 + x^2} \right\rangle. \tag{10}$$

If we transform to momentum space, v_2 is defined is a similar way [10], namely

$$v_2 = \left\langle \frac{p_x^2 - p_y^2}{p_x^2 + p_y^2} \right\rangle, \tag{11}$$

in which the same coordinate system is used as in figure 2. This similarity applies for all eccentricities, showing a clear connection between the shape of the interaction volume and the anisotropic flow.

3.1 Analysis Flow

The hydrodynamic flow is induced by the geometry of the collision and the electromagnetic fields, and can be calculated using measured properties from the outgoing particles. Within an event, an average is taken over certain azimuthal correlations, after which we average over all events. The variables used in the calculations are the outgoing azimuthal angles of the particles. A single particle cannot provide a value for the flow. For that reason, correlations between 2, 4, 6, and 8 particles are used to provide the value. For the 2 particle correlation, all possible sets of 2 particles have been made, for the 8 particle correlation, all possible sets of 8 particles, and so on. First, the cumulants $c_2\{2\}$, $c_2\{4\}$, $c_2\{6\}$, and $c_2\{8\}$ are defined:

$$\begin{aligned} c_2\{2\} &= \left\langle\left\langle e^{i2(\phi_1-\phi_2)}\right\rangle\right\rangle = \left\langle v_2^2 + \delta_2\right\rangle, \\ c_2\{4\} &= \left\langle\left\langle e^{i2(\phi_1-\phi_2-\phi_3-\phi_4)}\right\rangle\right\rangle - 2\left\langle e^{i2(\phi_1-\phi_2)}\right\rangle^2, \\ &= \left\langle v_2^4 + \delta_4 + 4v_2^2\delta_2^2\right\rangle - 2\left\langle v_2^2 + \delta_2\right\rangle^2, \\ &= \left\langle -v_2^4 + \delta_4\right\rangle, \\ &\dots \end{aligned} \tag{12}$$

The inner brackets denote the average over all particles, the outer brackets the average over all events. The angles ϕ_i are the azimuthal angles of the outgoing particles. The azimuthal correlation between the particles, independent of the reaction plane, is denoted by δ_2, which is also known as non-flow. These equations follow from the assumptions $\langle\delta_2^2\rangle = \langle\delta_2\rangle^2$, $\langle v_2^4\rangle = \langle v_2^2\rangle^2$ and that v_2 and δ_2 are uncorrelated. In other words, we have neglected the event-by-event fluctuations in v_2 and δ_2 [2]. Using some algebra, the following expressions are obtained

$$\begin{aligned} v_2\{2\} &= \sqrt{\langle v_2^2\rangle}, \\ v_2\{4\} &= \sqrt[4]{\langle v_2^4\rangle - 2\langle v_2^2\rangle^2}, \\ v_2\{6\} &= \sqrt[6]{\frac{1}{4}\left(\langle v_2^6\rangle - 9\langle v_2^2\rangle\langle v_2^4\rangle + 12\langle v_2^2\rangle^3\right)}, \\ v_2\{8\} &= \sqrt[8]{\frac{1}{33}\left(144\langle v_2^2\rangle^4 - 144\langle v_2^2\rangle^2 + 18\langle v_2^4\rangle^2 + 16\langle v_2^2\rangle\langle v_2^6\rangle - \langle v_2^8\rangle\right)}. \end{aligned} \tag{13}$$

Note that the model can track the azimuthal angle of a particle, and using equation 12, can determine $\langle v_2^2\rangle$, $\langle v_2^4\rangle$, ... Using these averages, equation 13 will give approximations of v_2. For the analysis of v_3, cumulants $c_3\{2\}$, $c_3\{4\}$, $c_3\{6\}$, $c_3\{8\}$ are defined by the complex e-powers $c_3\{2\} = \langle\langle\exp(i3(\phi_1 - \phi_2))\rangle\rangle$, ... The same expressions for the calculation of $v_3\{2\}$ to $v_3\{8\}$ are used as for v_2 (see equation 13).

4 The AVFD model

At RHIC and LHC, the interpretation of the signals measured suffer from background noise, which makes it hard to separate the properties of the QGP. The challenge is therefore to make the distinction between the corresponding signal of a given analysis and the background. For this reason, a framework/model has been created called Analous-Viscous Fluid Dynamics (AVFD). This model describes the initial state of the collisions using a Glauber prescription, and accounts for the development of the early stage elecromagnetic fields as well as for the propagation of anomalous fermion currents [4]. It implements the anomalous fluid dynamics to describe the fermion currents in QGP, on top of the neutral bulk background described by the VISH2+1 hydrodynamic simulations for heavy ion collisions [9]. The VISH2+1 is a code package that describes the evolution of a neutral charge QGP. VISH2+2 is coupled to a hadron cascade model, called UrQMD. UrQMD (Ultra Relativistic Quantum Molecular Dynamics) is a model for the description of hadron-hadron, hadron-nucleus and nucleus-nucleus collisions, developed at Frankfurt Institute for Advanced Studies.
In the AVFD model, the RH and LH fermion currents are described as perturbations on top of the expanding bulk matter [9] by the following equation:

$$\hat{D}_\mu J^\mu_{\chi,f} = \chi \frac{N_c Q_f^2}{4\pi^2} E_\mu B^\mu, \tag{14}$$

where $\chi = \pm 1$ which labels the chirality (RH/LH currents). f labels u, d quarks, Q_f is the electric charge, and $N_c = 3$. E_μ and B^μ are the external electromagnetic fields, given by $E_\mu = F^{\mu\nu}u_\nu$ and $B^\mu = \frac{1}{2}\epsilon^{\mu\nu\alpha\beta}u_\nu F_{\alpha\beta}$, $F^{\mu\nu}, F_{\alpha\beta}$ being the electromagnetic field tensor. $\hat{D}_\mu$ is the covariant derivate. The other fluid dynamical equations used for the evolution of the fermion currents are

$$\begin{aligned} J^\mu_{\chi,f} &= n_{\chi,f}u^\mu + \nu^\mu_{\chi,f} + \chi\frac{N_c Q_f^2}{4\pi^2}\mu_{\chi,f}B^\mu, \\ \Delta^\mu_\nu \hat{d}\left(\nu^\nu_{\chi,f}\right) &= -\frac{1}{\tau_r}\left[\left(\nu^\mu_{\chi,f}\right) - \left(\nu^\mu_{\chi,f}\right)_{NS}\right], \\ \left(\nu^\mu_{\chi,f}\right)_{NS} &= \frac{\sigma}{2}T\Delta^{\mu\nu}\partial_\nu\left(\frac{\mu_{\chi,f}}{T}\right) + \frac{\sigma}{2}Q_f E^\mu, \end{aligned} \tag{15}$$

where $n_{\chi,f}$ are the fermion densities and $\mu_{\chi,f}$ the corresponding chemical potential. σ is the diffusion coefficient and $\nu^\mu_{\chi,f}$ the 2nd-order of gradient expansion by incorporating relaxation evolution toward Navier-Stockes form [4, 9]. These equations are solved using Monte-Carlo integration using specific initial conditions. The solutions provide a description of the space-time evolution of the fermion currents.
After a given time, as the temperature drops, the QGP hadronizes. The temperature corresponding to this moment is called the freeze-out temperature T_f. The hadrons are produced in all fluid cells on the freeze-out hyper-surface. This process is governed by the Cooper-Frye formula

$$E\frac{\mathrm{d}N}{\mathrm{d}^3p}\left(x^\mu, p^\mu\right) = \frac{g}{(2\pi)^3}\int_{\Sigma_{fo}} p^\mu d^3\sigma_\mu f\left(x,p\right). \tag{16}$$

The combination of the solutions to equations 15 and the Cooper-Frye formula, provide the momentum distribution of the hadrons. At RIHC and LHC, this distribution will be measured.

The magnetic field is one of the most crucial components for the outgoing signal. The spectator nucleons have the largest contribution to the magnetic field. For that reason, the atomic number of the ions has great influence on the field. The centrality of a collision determines the amount of spectator nucleons, making the magnetic field evolution different for all centralities. In the model, the magnetic field decreases as follows:

$$B\left(\tau, x\right) = \frac{B_0}{1 + \tau^2/\tau_B^2}, \tag{17}$$

where τ_B is the magnetic field lifetime, and $B_0 = B(t = 0)$ the initial magnetic field. For Pb-Pb collisions, $\tau_B \approx 0.2$ fm/c. The magnetic field as a function of centrality is shown in figure 5. For central collisions, $\vec{B}$ is relatively small. As the collisions become more peripheral, the magnetic will increase in magnitude.

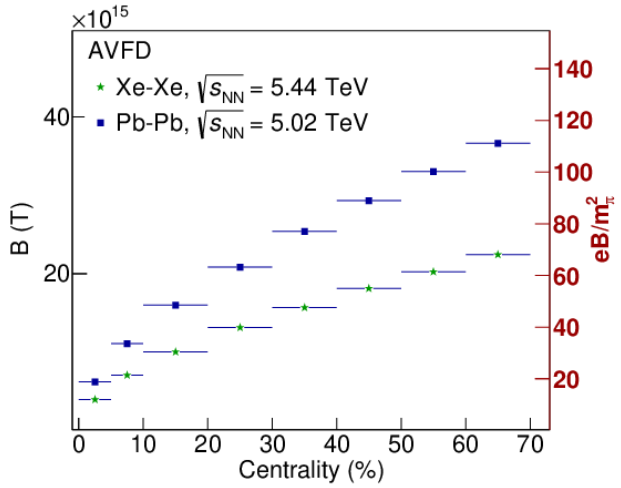

Figure 5: The magnetic field is plotted as a function of centrality for Pb-Pb and Xe-Xe collisions by the AVFD model. On the left y-axis, the magnitude of the magnetic field is shown. On the right y-axis, the magnetic field is scaled by the elementary charge and the mass of a pion squared. The figure is taken from Ref. [4].

The model was first calibrated, excluding CME (Chiral Magnetic Effect) or LCC (local charge conservation) effects. The input parameters that describe the centrality dependence of bulk measurements were tuned at various LHC energies. This will be referred to by 'Baseline'.

5 Results

Using the AVFD model, a total of 99900 events have been analysed from the Baseline. The events have been analysed for the different centrality intervals 0-5%, 5-10%, 10-20%, 20-30%, 30-40%, 40-50%, 50-60%, and 60-70%. For every event, the elliptic flow v_2 and triangular flow v_3 have been calculated. The center of mass energy of the collision is $\sqrt{s_{NN}} = 5.02$ TeV. The particles analysed are solely primary charged particles, i.e. charged particles which are directly created from the collision between the two Pb ions. As mentioned in section 3.1, the anisotropic flows need to be calculated using the cumulants. These cumulants result into expressions for $v_2\{2\}$, $v_2\{4\}$, $v_2\{6\}$, and $v_2\{8\}$ (the same correlations are used for v_3), which have been plotted in figure 6 for v_2 and in figure 9 for v_3. The model has been analysed two times, once for only positively charged particles, and once for negatively charged particles. Only particles with a transverse momentum p_t in range 0.2 to 5 GeV/c were analysed. This range is also used experimentally and is driven by the low efficiency at low values of p_t. This does not easily allow the extrapolation down to 0, and the need to have less contamination from non-flow (e.g. jets), which is dominant at higher values of p_t. All particles reside within pseudo-rapidity $\eta < 0.8$, thus matching the experimental coverage of ALICE.

I will continue by providing a brief summary of the work done by the writer to obtain the presented results. The Pb-Pb ion collisions have been modelled and the data has been generated using a Monte Carlo simulation (see section 4). Now, I have extracted the data and converted this data to .ROOT files. Root is a data analysis framework developed at CERN. It is commonly used in the analysis of high-energy physics. The data files contained all properties of the products of a collision, to name a few: the mass, charge, azimuthal angle, rapidity, momentum. Using these properties, a framework of calculations could generate the elliptic and triangular flow along with a complete set of other quantities that will not be explained/analysed in this report. I made adjustments in this framework to select the positively or negatively charged particles. All calculated quantities were again stored in new result files. After the calculations, I wrote pieces of code that would extract and plot the elliptic and triangular flow from these result files.

5.1 Results Elliptic Flow v_2

Figure 6a presents the centrality dependence of elliptic flow v_2. Two sets of data are shown: the red markers show the values for v_2 of the positive charges, the blue markers show that of the negative charges. For both positve and negative charges, the value of v_2 is increasing progressively from central to peripheral collisions. At 50-60%, a maximum is reached, after which the values start to decrease. The reason for this centrality dependence is related to the geometry of the collision, which is controlled by the impact parameter. For central collisions, the geometry of the interaction volume of almost symmetric.

In figure 7a, the ratio between v_2 of the positively and negatively charged particles v_2^+/v_2^- has been plot as a function of centrality. In addition, a fit has been made in order to find a relation between the positive and negative particles. The fit used is a first order polynomial, i.e., a formula of shape $y = ax + b$, where a and b are constants. To measure the reliability and accuracy of the fit, the reduced chi square χ^2_ν test is used. The reduced chi square is a number that involves the fit value,

the data points and all deviations. If $\chi^2_\nu \approx 1$, the fit is considered 'good'. If $\chi^2_\nu \gg 1$ or $\chi^2_\nu \ll 1$, the current fit does not represent the data points well [11]. The fit for the ratio between the $v_2\{2\}$ values of positive and negative particles per centrality is $y = (-8.3 \pm 0.7) \cdot 10^{-4}x + (1.0 \pm 0.003)$. For this fit, $\chi^2_\nu = 8.1$.

For $v_2\{4\}$, some lower centralities are not filled due to numerical instabilities introduced by the low statistics sample (for this calculation) in the model. The shape of plot is similar to that of $v_2\{2\}$, although the negative particles reach the maximum at 40-50%, while the positive particles have the maximum at 50-60%. Figure 7b illustrates the v_2 ratio between the positive and negative particles. The fit is $y = (7.4 \pm 3.4) \cdot 10^{-4}x + (0.9 \pm 0.1)$, with $\chi^2_\nu = 8.28$. However, the uncertainty in the first term of the fit is approximately 50% of the estimated value. The slope of the fit is therefore not a reliable value.

Rather odd results appear in figure 6c, which describes correlation $v_2\{6\}$. The lowest centrality 0-5% is inconsistent with the other centralities. Not only exceeds the value of the positive particles the negative, but the value is higher than 5-10%. In addition, the v_2 of the negative particles at 60-70% is higher than v_2 at 50-60%. The graph of the positive particles is very similar to $v_2\{2\}$. The v_2 ratio has again been plot and the fit in figure 7c. For the $v_2\{6\}$ correlation, the fit is $y = (-4.9 \pm 5.1) \cdot 10^{-4}x + (0.97 \pm 0.02)$. Again, the uncertainty in the slope of the fit is too high to made any reasonable conclusion.

In figure 6d, we observe the correlation $v_2\{8\}$. The shape of this graph is very consistent with the shape of $v_2\{6\}$. The data points follow the trend $y = (-10 \pm 87) \cdot 10^{-5}x + (0.97 \pm 0.03)$, with $\chi^2_\nu = 0.0887$. For this correlation, we have to conclude that the slope of the fit is too uncertain to draw a conclusion.

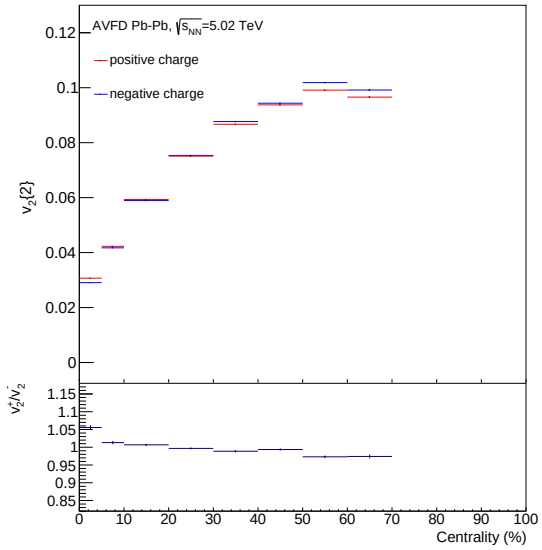

(a) $v_2\{2\}$

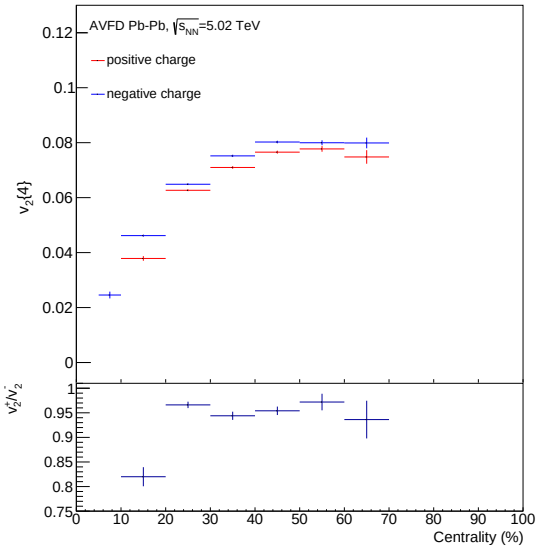

(b) $v_2\{4\}$

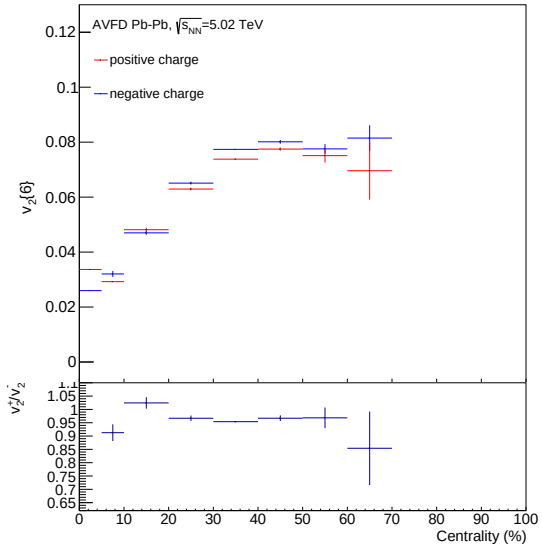

(c) $v_2\{6\}$

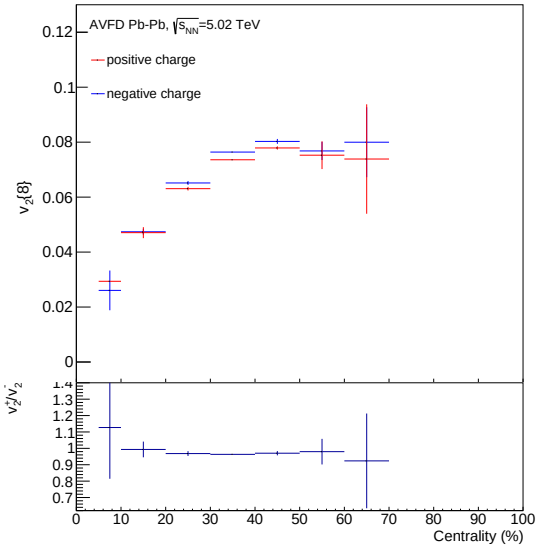

(d) $v_2\{8\}$

Figure 6: All v_2 correlations as a function of centrality for Pb-Pb collisions from the AVFD model at $\sqrt{s_{NN}} = 5.02$ TeV. In addition, the ratio of the v_2 values between the positively (v_2^+) and negatively (v_2^-) charged particles is shown.

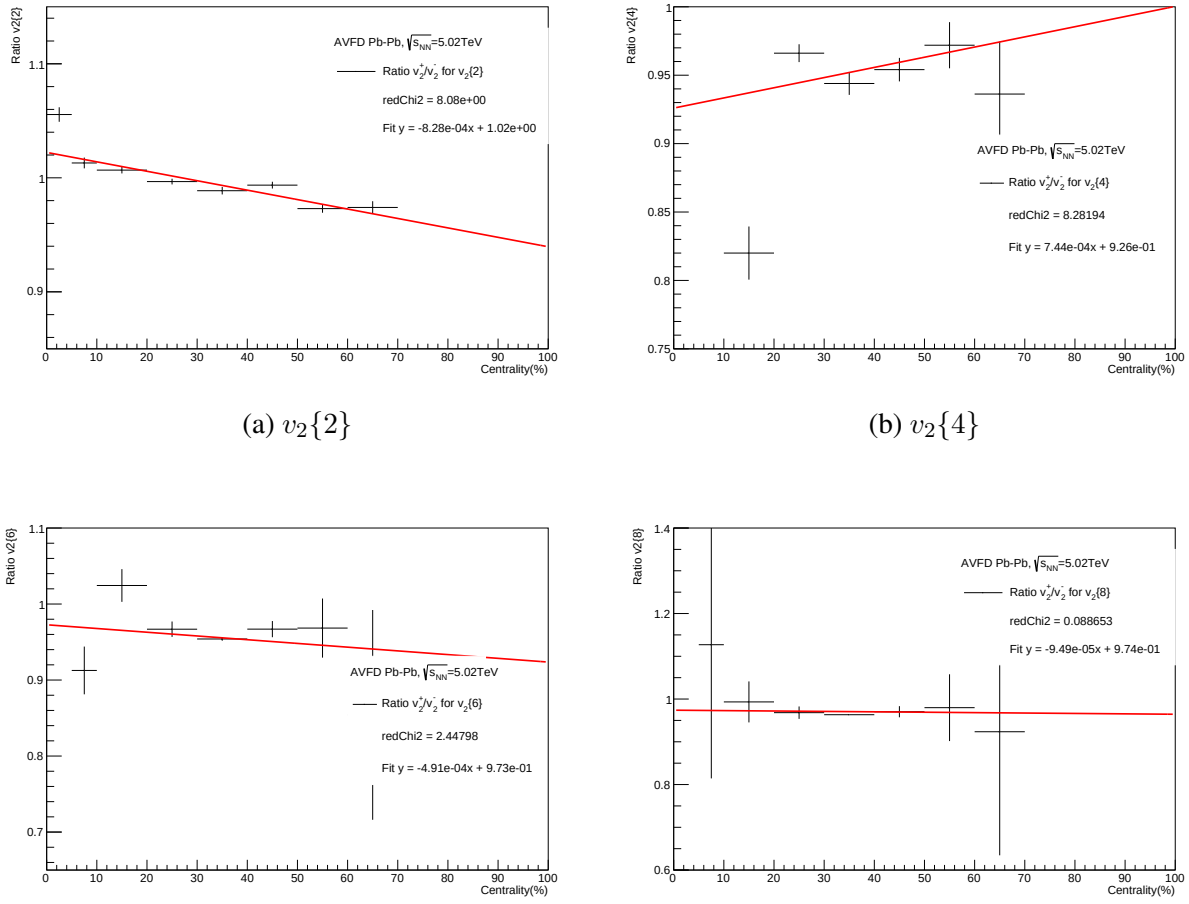

(a) $v_2\{2\}$ (b) $v_2\{4\}$

(c) $v_2\{6\}$ (d) $v_2\{8\}$

Figure 7: The ratio of v_2 between the positve and negative particles of all v_2 correlations as a function of centrality for Pb-Pb collisions from the AVFD model at $\sqrt{s_{NN}} = 5.02$ TeV.

It can be seen from the 2 and 4 particle correlations that the results for positive and negative charges are not fully compatible. The non-flow effect are not likely to be the source for this incompatibility. The outgoing positive and negative hadrons, measured as jets, share their correlations. Furthermore, if neutral particles decay, equally positive as negative charge is produced. The non-flow effects do not have a charge dependence. This indicates that another element of the collisions causes the difference between positive and negative charges. The proposition is therefore that the influence of the early stage magnetic field affects the motion of the final state particles.
Now, let us recall that the centrality is characterised by the fraction $\pi b^2/\pi(2R_A)^2$. For peripheral collisions, the impact parameter increases and therefore the centrality too. Furthermore, the elliptic flow is defined by the average cosine of the azimuthal angle minus the reaction plane by

$$v_2(p_t, y) = \langle \cos\left[2\left(\phi - \Psi_{RP}\right)\right] \rangle. \tag{18}$$

The average is taken over all events. The impact parameter equals zero for central collisions. The two heavy ions will collide head on and the interaction volume of the collision will be nearly symmetrical in the y-axis. The assumption is made that the protons and neutrons are homogeneously

distributed in the heavy Pb ions. The 'top' or 'back' will not contain more protons than the 'bottom' or 'front'. Using the symmetry of the interaction volume, it can be argued that the product particles will not have a preferred outgoing direction during and after the collision. For a central collision, the processes that occur at positive y, will also occur at equal negative y and the outgoing particles will, on average, equal. Using equation 18 and the argument above, the average cosine of the outgoing particles with respect to the reaction plane (for central collisions, Ψ_{RP} is on the x-axis) will approach zero. The fluctuations in the position of the nucleons result in a value for v_2, though this value is significantly smaller than v_2 for peripheral collisions. For nonzero impact parameter b, an energy shift will occur from the y-axis. This shift will result into a flow. The greater b, the greater this shift or flow will be, until the impact parameter is too large for the particles to interact. In other words, the elliptic flow increases as the centrality increases for small centralities and will decrease for large centralities. We observe that the maximum of this flow is around 50-60% centrality for $v_2\{2\}$ and $v_2\{4\}$, and around 40-50% centrality for $v_2\{6\}$ and $v_2\{8\}$ in figure 6.

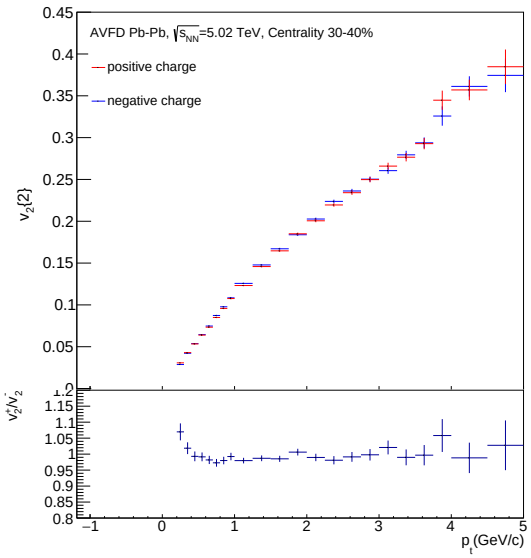

Figure 8: $v2\{2\}$ is plot as a function of p_t at centrality 30-40% for a Pb-Pb collision from the AVFD model at $\sqrt{s_{NN}} = 5.02$ TeV for positive and negative particles.

In figure 8, the p_t-differential elliptic flow is plotted, meaning v_2 as a function of transverse momentum p_t for an indicative centrality of Pb-Pb collision, i.e. 30-40%. Let us recall that p_t is the momentum times the sine of the emission angle in the stationary frame of the source. The elliptic flow is strictly increasing in the p_t range 0 to 5 GeV/c. The ratio between the positive and negative particles has been plotted right underneath in fig 8. It can be seen that the two results are consistent within the current uncertainties for $p_t > 0.7$ GeV/c. For lower values of transverse momentum, the v_2 for positive particles starts to become larger than the one for negative particles. This plot shows how the electromagnetic fields influences the flow and that the flow is very dependent on the transverse momentum. The electromagnetic field has a notable different influence on the positive and negative particles, although the difference does not seem very significant for higher values of p_t.

5.2 Results Triangular Flow v_3

The results for v_3 as a function of centrality are shown in figure 9. However, a number of errors can be observed for v_3. The correlation $v_3\{4\}$ is only filled for two centralities and negative charge. $v_3\{6\}$ contains a few more data points, but not enough to draw any conclusions from. The same reasoning applies for $v_3\{8\}$. The cause for these graphs is the difficulty that the AVFD model has with calculating v_3. Only $v_3\{2\}$ provides a result for all centralities.
For flow $v_3\{2\}$, the same increasing shape for central collisions, and slightly decreasing for peripheral collisions as v_2 is shown is figure 9a. The ratio v_3^+/v_3^- is decreasing, which is agreement with $v_2\{2\}$. As for v_2, the ratio has been fit in figure 10. The corresponding formula is $y = -(1.2 \pm 0.2) \cdot 10^{-3}x + (1.05 \pm 0.005)$, with $\chi^2_\nu = 1.37$. Both the charge-even v_2 and the charge-odd v_3 are increasing as a function of centrality and the ratios v_2^+/v_2^- and v_3^+/v_3^- are both decreasing. The main observable difference is the magnitude of the flow. The electromagnetic field has a similar impact on the the flows and their ratios.
Elliptic flow v_2 has larger values than the triangular flow, making it easier to measure. Furthermore, for both v_2 and v_3, the 6 and 8 particle correlations contain higher uncertainties, or bins are not filled at all (for v_3). These are statistically less accurate, since one would need more events to simulate the same accuracy for the possible sets of 6 or 8 particles. Furthermore, if we recall equation 13, terms underneath the 4th, 6th or 8th root can be negative, making values at certain centralities for $v_3\{4\}$, $v_3\{6\}$ and $v_3\{8\}$ nonexistent.

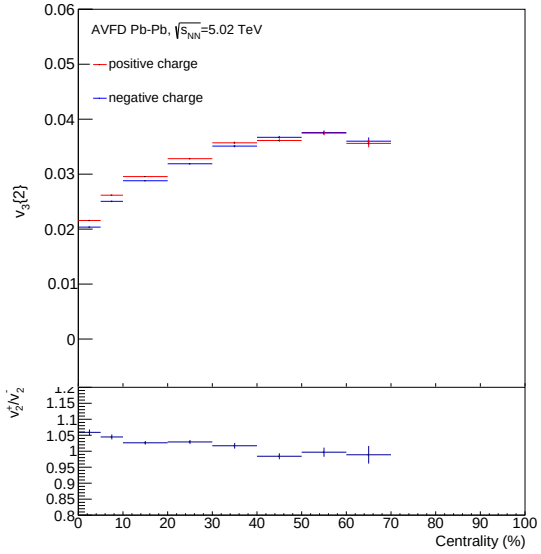

(a) $v_2\{2\}$

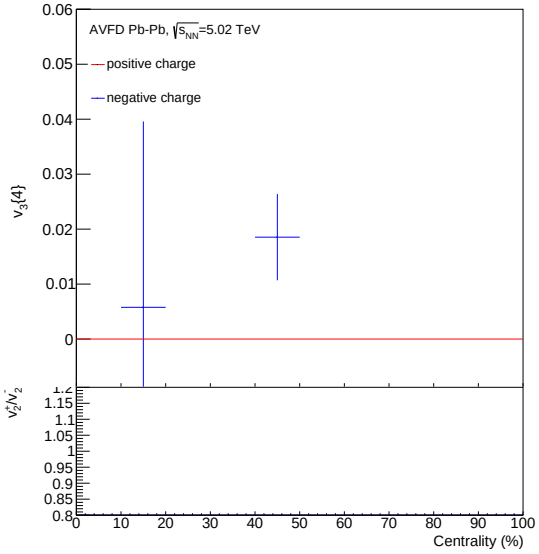

(b) $v_2\{4\}$

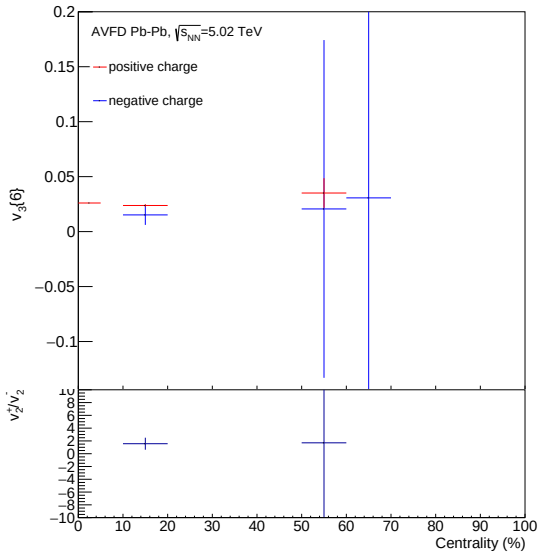

(c) $v_2\{6\}$

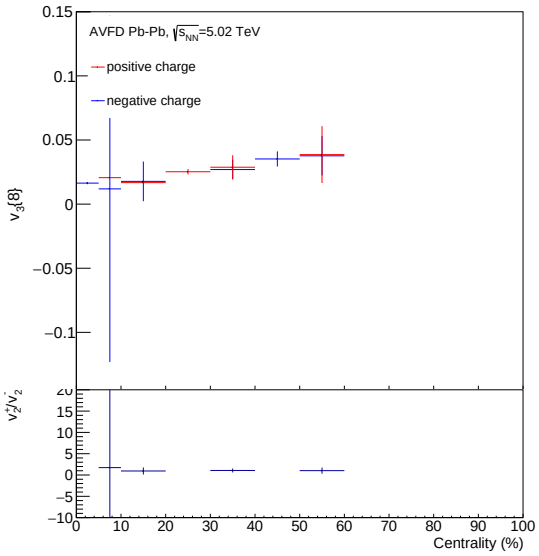

(d) $v_2\{8\}$

Figure 9: All v_3 correlations as a function of centrality for Pb-Pb collisions from the AVFD model at $\sqrt{s_{NN}} = 5.02$ TeV. In addition, the ratio of the v_3 values between the positively (v_3^+) and negatively (v_3^-) charged particles is shown.

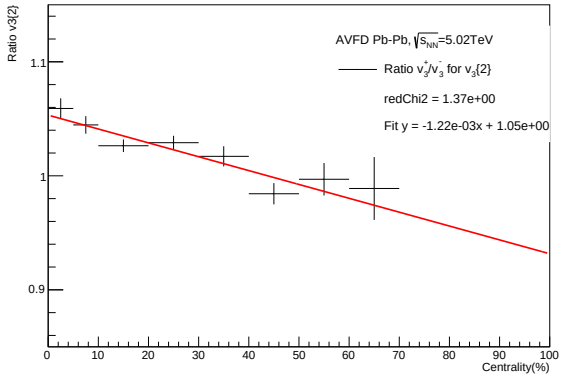

Figure 10: $v_3\{2\}^+/v_3\{2\}^-$ is plot as a function of centrality for a Pb-Pb collision from the AVFD model at $\sqrt{s_{NN}} = 5.02$ TeV. A first order polynomial fit is made.

The transverse momentum p_t is plot as a function of v_3 in figure 11. The magnitude of v_3 is strictly increasing. The ratio v_3^+/v_3^- as a function of p_t fluctuates right underneath 1. For low p_t, the positive particles tend to have a greater triangular flow. In this range, the two charges are not compatible. For $p_t \in [1, 4]$, the positive and negative charges do seem to be compatible. This result is in agreement with the result for v_2.

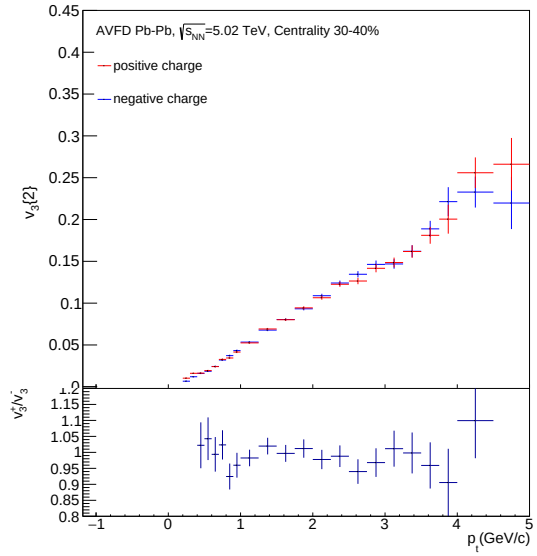

Figure 11: $v_3\{2\}$ is plot as a function of p_t at centrality 30-40% for a Pb-Pb collision from the AVFD model at $\sqrt{s_{NN}} = 5.02$ TeV for positive and negative particles.

6 Conclusion

In section 2.2, we found that the electromagnetic fields in a heavy-ion collision arise from four forces/laws: Faraday's law, Lorentz force, Coulomb force, and the QGP. The latter is the deconfined state of quarks and gluons, in which magnetic fields up to 10^{15} Tesla are induced. The magnitude of these magnetic fields is determined by the size of the ions, the center of mass energy, the centrality of the collision (see figure 3), and the electric conductivity σ of the QGP. The magnitude of the magnetic field decreases over time, as depicted in figure 4. The early stage of the magnetic field is believed to have effect on the final particles distribution (see section 3).
The influence of the magnetic field was tested using the AVFD model. This model simulates the heavy-ion collisions using a set of anomalous-viscous fluid dynamical equations for the expansion of the QGP. This set is solved by Monte Carlo integration using an appropriate set of initial conditions. In this model, a magnetic field of the form $B = B_0/(1+\tau^2/\tau_B^2)$ is used. Using the azimuthal angle of the outgoing hadrons, the cumulants c_2 and c_3 could be constructed, followed by estimates for v_2 (elliptic flow) and v_3 (triangular flow) using 2, 4, 6, and 8 particle correlations. The elliptic and triangular flow describe the anisotropical expansion of the QGP. The interaction volume is described as a combination of different shapes, with an ellipse being the second and a triangle being the third. The eccentricities of these shape are associated with the flow coefficient of this shape.
I analysed the model twice. Once filtering only positive charges, and once only negative. Both charges produce an elliptic and triangular flow, of which I have plotted the ratio v_2^+/v_2^- and v_3^+/v_3^- as a function of centrality. These figures are shown in section 5. I found that the elliptic flows of positive and negative charges for 2 and 4 particle correlations are not compatible. Since non-flow effect are not charge dependent, the proposition is made that the early magnetic field influences the positive and negative charges differently in the QGP. This influence is then observed by the final hadrons. For the 6 and 8 particle correlations, v_2^+ and v_2^- seem to be compatible. The model only fully computed the 2 particle correlation for v_3. These results of the positive and negative charges are not compatible either. At last, the elliptic and triangular flow have been plot as a function of transverse momentum p_t. For the elliptic and triangular flow, the positive and negative charges are compatible in the p_t range 0.7 to 5 GeV/c for v_2, and in range 1 to 4 GeV/c for v_3.
When thinking about further studies, one can study higher harmonics and the influence of v_4, v_5 and so on. Also, the parity-violating effects in QCD can be studied using the AVFD model. If the hypothesis is right, these studies will be groundbreaking.

References

[1] R. S. Bhalerao, in *1st Asia-Europe-Pacific School of High-Energy Physics* (2014), 1404.3294.

[2] R. Snellings, New Journal of Physics **13** (2011), URL https://doi.org/10.1088/1367-2630/13/5/055008.

[3] V. V. Skokov, A. Y. Illarionov, and V. D. Toneev, International Journal of Modern Physics A **24**, 5925 (2009), URL https://doi.org/10.1142/S0217751X09047570.

[4] P. Christakoglou, S. Qiu, and J. Staa, *Systematic study of the chiral magnetic effect with the avfd model at lhc energies* (2021), 2106.03537.

[5] A. Bilandzic, R. Snellings, and S. Voloshin, Physical Review C **83** (2011), ISSN 1089-490X, URL http://dx.doi.org/10.1103/PhysRevC.83.044913.

[6] U. Gürsoy, D. Kharzeev, E. Marcus, K. Rajagopal, and C. Shen, Phys. Rev. C **98**, 055201 (2018), URL https://link.aps.org/doi/10.1103/PhysRevC.98.055201.

[7] L. McLerran and V. Skokov, Nuclear Physics A **929**, 184 (2014), ISSN 0375-9474, URL https://www.sciencedirect.com/science/article/pii/S0375947414001237.

[8] H.-T. Ding, A. Francis, O. Kaczmarek, F. Karsch, E. Laermann, and W. Soeldner, Phys. Rev. D **83**, 034504 (2011), URL https://link.aps.org/doi/10.1103/PhysRevD.83.034504.

[9] S. Shi, Y. Jiang, E. Lilleskov, and J. Liao, Annals of Physics **394** (2018), ISSN 0003-4916, URL https://www.sciencedirect.com/science/article/pii/S0003491618301131.

[10] R. S. Bhalerao et al., PLB 627, 49 (2005).

[11] P. van Capel, *Dictaat Data-acquisitie & Toegepaste analyse, Data-V* (Universiteit Utrecht, 2017).